J Bio Tribo Corros (2015) 1:19
DOI 10.1007/s40735-015-0019-7

ORIGINAL PAPER

Synthesis, Characterization and Anticorrosion Studies of New Homobimetallic Co(II), Ni(II), Cu(II), and Zn(II) Schiff Base Complexes

A. M. Nassar[1] · A. M. Hassan[1] · M. A. Shoeib[2] · A. N. El kmash[1]

Received: 14 March 2015 / Revised: 10 May 2015 / Accepted: 4 June 2015 / Published online: 12 June 2015

Abstract New homobinuclear Co(II), Ni(II), Cu(II), and Zn(II) complexes with Schiff base (**H_2L,1**) have been synthesized and investigated using physicochemical techniques viz. IR, ^{1}H NMR, ^{13}C NMR, ESR, UV–Visible spectrometric methods, thermal gravimetric analysis, and magnetic moment measurements. The corrosion inhibition studies of the compounds on mild steel in (0.5 M) HCl have been investigated by weight loss, potential dynamics polarization, and scanning optical microscope. The adsorption of compounds was founded to obey the Langmuir adsorption isotherm model showing mixed type inhibition behavior. The in vitro antibacterial studies of the complexes against sulfate-reducing bacteria proved them as growth inhibiting agents.

Keywords Schiff base · Binuclear complexes · Mild steel · Acid solution · Polarization · Microbiological corrosion

1 Introduction

Corrosion is the destructive attack of metals by its environment and destruction of metal due to heterogeneous chemical reaction which is called the chemical corrosion [1]. The mild steel has wide applications in various industries as construction materials for reactors, heat exchange, boilers, storage tanks, and oil and gas transport pipelines due to its mechanical properties and low cost [2]. The use of corrosion inhibitors is one of the most practical methods for the protection of metals against corrosion in acidic media [3]. The interaction between the metal surface and hetero atoms like nitrogen, oxygen, and sulfur plays an important role in the corrosion inhibition due to the free electron pairs that possess [4–7]. Moreover, the compounds that contain π bonds generally exhibit good inhibition efficiency supplying electrons via the π-orbitals [8]. Due to the presence of azomethane (C=N) group in the Schiff base molecules, they should be good corrosion inhibitors. Some Schiff bases and transition metal complexes have been reported as effective corrosion inhibitors for mild steel, aluminum, copper, and zinc in acid media [9–15]. The effect of diacetylmonoxime derivative on the corrosion of metal in acidic media was reported [16]. Much corrosions of industrial equipments have been ascribed to microbiologically influenced corrosion (MIC) [17]. Sulfate-reducing bacteria (SRB) are the main reason to cause the MIC by accelerating corrosion rate, inducing stress corrosion, and pitting corrosion [18]. The biocides can be used as SRB growth inhibitors to protect the metals from microbial corrosion [19].

In this study, we synthesized and characterized Cobalt(II), Nickel(II), Copper(II), and Zinc(II) complexes with Schiff base; Bis(diacetylmonoxime)biphenyl-3,3′-dimethoxy-4,4′-diamine Schiff base (**H_2L,1**) which is synthesized from the condensation of o-Dianisidine with Diacetylmonoxime and studied the effect of the compounds as corrosion inhibitors of carbon steel in 0.5 M HCl. The gravimetric and electrochemical techniques such as weight loss and potentiodynamic polarization measurements were used in this study. The scanning optical

✉ A. M. Nassar
nassar_tanta@yahoo.com

[1] Chemistry Department, Faculty of Science, Al-Azhar University, Nasr City, Cairo, Egypt

[2] Central of Metallurgical Research and Development Institute (CMRDI), Cairo, Egypt

microscope was used to explain adsorption of inhibitors on the surface of metal. Some isotherm was used to describe the adsorption behavior of the compounds understudied. Also, antibacterial activity against SRB of compounds was studied.

2 Experimental

2.1 Materials and Methods

The analytical reagent grade (AR) o-Dianisidine, Diacetylmonoxime, $CoCl_2{\cdot}6H_2O$, $NiCl_2{\cdot}6H_2O$, $CuCl_2{\cdot}2H_2O$, $ZnCl_2{\cdot}2H_2O$ are Aldrich or Merck chemicals. Organic solvents used (methanol, ethanol, diethyl ether, and acetone) were HPLC or extra-pure grades and were used without further purification. The electrolyte solution was 0.5 M HCl, prepared from analytical grade HCl and distilled water. All corrosion tests were performed at room temperature. The mild steel working electrode specimens have the following composition, C = 0.066 %, Mn = 0.3 %, P = 0.01 %, S = 0.02 %, Cr = 0.026 %, Cu = 0.02 %, and Fe = 99.5 % and using 2 cm^2 coupons of same sample material. The weight loss and Polarization measurements were performed on mild steel in deaerated 0.5 M HCl solution with and without Schiff base and its complex additives within the concentration ranges 1, 3, 5, and 7×10^{-4} Mol/dm^3. Weight loss experiments were carried out electronically at room temperature. After recording the initial weights of mild steel specimens on a Mettler Toledo, Japan AB 135-S/FACT, single pan analytical balance, (with a precision of 0.01 mg), they were kept in different isolated chamber (perfectly insulated from each other) for 48 h of exposure time in different concentrations 1, 3, 5, 7×10^{-4} Mol/dm^3. A uniform thin film of compounds was adsorbed on to the metal coupons after 48 h of exposure. Then these coupons were taken out from the chamber and washed initially under the running tap water. Loosely adhering corrosion products were removed with the help of rubber cork and the specimen was again washed thoroughly with triple distilled water and acetone and dried with hot air blower and then weighed again. The electrochemical behavior of the mild steel sample in inhibited and non-inhibited solution was studied by recording anodic and cathodic potentiodynamic polarization curves. Measurements were performed in the 0.5 M HCl solution containing different concentrations of the tested inhibitor by changing the electrode potential automatically from −250 to +500 mV versus corrosion potential at a scan rate of 1 mV s^{-1}. The Stock solutions of the Schiff base and its complexes were made in 10:1 ratio of water: DMF mixture by volume to ensure solubility. The optical microscope images were taken to establish the interaction of inhibitors with metal surface in acid medium. The surface images of carbon steel samples were examined by optical microscope after the sample is immersed in 0.5 M HCl for 48 h in the absence and presence of inhibitors. The antibacterial activity of compounds was carried out at National Research Center (NRC). The incubation period was for seven days at 30 °C.

2.2 Instruments

Elemental analysis (% C, % H, and % N) and mass spectra were determined in the Micro Analytical Laboratory. Magnetic susceptibility measurements were carried out at room temperature on a Sherwood Scientific Magnetic Balance. Electronic spectra were measured in range (195–1100 nm) using a Perkin-Elmer lambda 35 UV–Vis Spectrometer. Infrared (IR) spectra were recorded using KBr pellets on a Perkin-Elmer 1430 Spectrometer for the region (200–4000 cm^{-1}). ^1H NMR and ^{13}C NMR spectra were recorded on GEMINI-300BB NMR 500 MHz spectrometer. The thermo gravimetric analysis (TGA) for complexes were obtained at a heating rate of 10 °C/min and flowing nitrogen atmosphere over a temperature range of 20–800 °C. The electron spin resonance (ESR) spectra were recorded on Bruker EMX spectrometer working in expand 9.7 GHz with 100 kHz frequency and microwave power 1 MW and modulation amplitude 4Gauses. Potentiodynamics polarization measurement was carried out using Autolab-PGSTAT302 N-HP and using a glassy carbon working electrode, platinum wire auxiliary electrode, and an Ag/AgCl as reference electrode and Scanning Optical Microscope (SOM) using ZEISS, Axiovert 40 mat microscope.

2.3 Synthesis of Schiff Base Ligand H_2L,1

Ligand (L) is prepared by mixing (2:1) molar ratio of diacetylmonoxime (1.011gm, 0.01 mol) and o-dianisidine (1.22 g, 0.005 mol) in 50 ml hot etathanol solution and refluxing the mixture for 3 h with continous stirring. Upon cooling, black oily residue that remains is treated with petroleum ether(20 ml) with vigorous stirring for 30 min. The contents are collected in beaker and allowed to form precipitate. The obtained black precipitate was filtered off, and recrystallized from DMF to give deep brown crystals. Finally the crystals were washed several times with diethyl ether and then air dried. The purity of the ligand was checked by TLC technique. M.p. 155 °C, M. Wt. 410.4, Yield (81.2 %), Anal. Calc. for $C_{22}H_{26}N_4O_4$: C, 64.39; H, 6.34; N, 13.65 %, Found: C, 64.47; H, 6.27; N, 13.84 %; main IR Peaks (KBr, cm^{-1}): ν(OH)3441, ν(C=N)1620.

2.4 Synthesis of the Metal Complexes

A sample of hydrated MCl_2 (M = Co, Ni, Cu, and Zn) (2.0 mmol) was dissolved in hot ethanol solution (30 ml), and was added to an ethanolic (30 ml) solution of **H_2L** (1.0 mmol). The reaction mixture was heated under reflux for 3 h. The fine solid complexes formed were collected by filtration, washed with hot ethanol, hot water, and ether, and then, air dried. The complexes are stable in air.

*2.4.1 The Complex, $Co_2L(H_2O)_2(Cl)_2{\cdot}2H_2O$ (**2**)*

Dark brown solid. M.p >300 °C; M. Wt. 670.9; Anal. Calc for $C_{22}H_{34}Co_2N_4O_8Cl_2$: C,39.34; H,5.06; N,8.34; Co, 17.58 %; Found: C, 39.5; H, 5.12; N, 8.4; Co, 16.9 %; main IR Peaks(KBr, cm^{-1}): ν(C=N) 1608.

*2.4.2 The Complex, $Ni_2L(H_2O)_2(Cl)_2{\cdot}2H_2O$ (**3**)*

Dark brown solid. M.p >300 °C; M. Wt. 670.38; Anal. Calc for $C_{22}H_{34}Ni_2N_4O_8Cl_2$: C,39.38; H,5.07; N,8.35; Ni, 17.5 %; Found: C, 39.4; H, 5.14; N, 8.4; Ni, 17.0 %; main IR Peaks(KBr, cm^{-1}): ν(C=N) 1608.

*2.4.3 The Complex, $Cu_2L(H_2O)_2(Cl)_2{\cdot}2H_2O$ (**4**)*

Black solid. M.p.295 °C; M. Wt. 680.8; Anal. Calc for $C_{22}H_{34}Cu_2N_4O_8Cl_2$: C,38.8; H,4.99; N,8.23; Cu, 18.68 %; Found: C, 38.9; H, 5.03; N, 8.29; Cu, 17.9 %; main IR Peaks(KBr, cm^{-1}): ν(C=N) 1598.

*2.4.4 The Complex, $Zn_2L(H_2O)_2(Cl)_2{\cdot}2H_2O$ (**5**)*

Brown solid. M.p > 300 °C; M. Wt. 683.8; Anal. Calc for $C_{22}H_{34}Zn_2N_4O_8Cl_2$: C,38.6; H,4.97; N,8.2; Zn, 19.1 %; Found: C, 38.7; H, 4.96; N, 8.28; Zn, 18.9 %; main IR Peaks(KBr, cm^{-1}): ν(C=N) 1610.

2.5 Antibacterial Assay

The enrichment of (SRB) and biological assay was carried out using most probable number (MPN) technique [20].

3 Results and Discussion

The present Schiff base **H_2L**, Fig. 1 was prepared by refluxing an ehanolic solutions of o-dianisidine with diacetyl monoxime in (1:2) molar ratio, respectively. The structure of formed Schiff base was established by IR, ^1H and ^{13}C NMR, mass, and UV–Vis spectra as well as elemental analysis. All complexes were prepared by direct reaction of **H_2L** with metal chlorides in (1:2) molar ratio, respectively.

3.1 Characterization of Schiff Base Ligand (H_2L)

The infrared spectrum of the Schiff base ligand **H_2L** in the region 200–4000 cm^{-1} shows a medium absorption band at 1620 cm^{-1} assigned to the ν(C=N) azomethine stretching vibrations, indicating the formation of the Schiff base linkage. Furthermore, the absence of C=O and NH_2 stretching vibration in the spectra of the ligand related to aldehyde and amine, respectively, indicate the occurrence of Schiff base condensation [21]. The band observed at 1504 cm^{-1} was assigned to ν(C=N) oxime [22]. The spectrum shows a broad medium intensity band that occurs at 3441 cm^{-1} which is assigned to the oxime NOH group. Also, the two weak bands at 2840–2960 cm^{-1} region can be taken as evidence for the presence of intramolecular hydrogen bond OH….N=C [23, 24]. As the hydrogen bond becomes stronger, the bandwidth increases, however, this band is sometimes not detected. Hydrogen bonds in these Schiff bases are usually very strong while the ligands are relatively planar with adequate intramolecular distance that favors intramolecular hydrogen bond formation. The methoxy groups as electron-donating groups increase the electron density on the hydroxyl oxygen making the H–O bond stronger; the absorption usually appears as a broad band in the IR spectrum. The two weak intensity bands at 3090 and 2860 cm^{-1} correspond to $\nu(C–H)_{ar}$ and $\nu(C–H)_{aliph}$ stretching vibrations. The stretching vibration observed at 1272 cm^{-1} is due to ν(C–O) [25]. Also, the strong band at 1030 cm^{-1} is assigned to ν(NO) oxime [26]. The (Ph–N) gives medium intensity band at 1122 cm^{-1}. The ^1H NMR spectrum (Fig. 2a, b) shows that signals lying at the range 11.3 ppm are due to the resonance hydroxyl groups; the signals of OH groups lying at the higher field side can be attributed to the contribution of the OH group intramolecular and intermolecular hydrogen bonds; the addition of D_2O to the previous solution results in the disappearance of the signal due to proton exchange [27]. Also, the multiple signals lying in the range of 6.6–7.2 ppm [28] are due to the resonance of aromatic protons. The methoxy groups protons appear signal at 3.8 ppm [29].

The ^{13}C NMR spectrum of the free ligand was recorded in DMSO-d6. The spectrum showed signals at 129 ppm (C1-ipso), 108 ppm(C2-H), 114 ppm(C3-H), 118 ppm(C4-ipso), 135 ppm(C5-ipso), 146.5(C6-ipso), 55 ppm(C9-H), and 38,40 ppm(C7 and C8). The electronic spectrum of the ligand displaying bands at 314 and 360 nm are attributed to intraligand π–π* and *n*–π* transitions for the benzene ring and azomethine group [30]. The mass spectrum of the free Schiff base ligand (Fig. 3) shows its molecular ion peak at

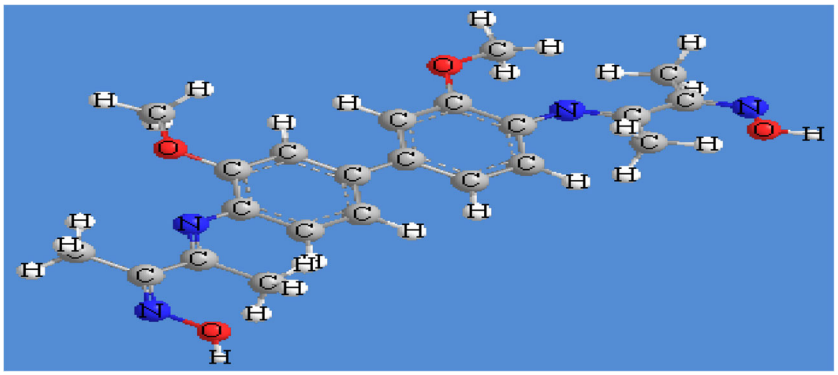

Fig. 1 The proposed Structure of Schiff base ligand $\mathbf{H_2L}$

m/e = 411 which matches with a formula weight (Scheme 1).

3.2 Characterization of Complexes

3.2.1 IR Spectra

The infrared spectra of the complexes were collected in a Table 1 and compared with that of free ligand to give some information about the bonding in the complexes. The band in the IR spectrum of the ligand at 1620 cm^{-1} is found to be shifted to lower frequencies 1598–1608 cm^{-1} in the spectra of the complexes, indicated donation of the lone pair of electrons on azomethine nitrogen to metal center [31]. Moreover the new band in the far infrared spectra of the complexes in the range 584–615 cm^{-1} is assigned to the νM–N. Deprotonation of all hydroxyl functions is confirmed by the lack of Oxime N–O–H and shift of νN–O to higher wave number to about 1059–1063 cm^{-1} but appeared in free ligand at 1030 cm^{-1}, indicating the participation with the metal ion as $–O^-$. The broadening bands observed in the spectra of complexes in the range 3377–3488 cm^{-1} considerable support the presence of water molecules in the complexes [24, 32, 33]. The weak bands appeared in the far IR spectra between 615–660 cm^{-1} were attributed to νM–O. The far infrared spectra of the complexes show weak bands in the range 312–318 cm^{-1} ascribable to νM–Cl.

3.2.2 UV–Vis Spectra

The electronic spectrum of Co(II) complex **2**, Fig. 4 shows low intensity shoulders at 569 and 670. The former bands are probably due to $^4A_2$ (F) → $^4T_1$ (P) and $^4A_2$ (F) → $^4T_1$ (F) which indicates the tetrahedral geometry of this complex. Magnetic moment (4.2 B.M) confirms the tetrahedral geometry of the ligand around Co^{+2} ions [34]. The spectrum of the Ni(II) complex **3** shows a very broad band at 520 nm containing the $^3T_1$(F) → $^3T_1$(P) which suggests that the coordination geometry at the metal atom could be distorted from the tetrahedral configuration of this complex. The magnetic moment (3.6 B.M) indicates the tetrahedral geometry [35]. The broad band at 528 nm in the spectrum of Cu(II) complex **4**, as well as the μ_{eff} value (1.85 B.M) is corresponding to the tetrahedral of the copper complex [36]. Finally, the electronic absorption spectrum of Zn(II) complex **5** shows an absorption band at 425 nm attributed to the LMCT transition, which is compatible with this complex having an tetrahedral structure; the diamagnetic behavior is due to d^{10} configuration of Zn^{+2} ions [37].

3.2.3 NMR (^1H and ^{13}C)

The ^{1}H NMR spectrum of the zinc complex **5** is recorded in DMSO-d6 at room temperature. In the spectrum of the zinc complex the hydroxyl oxime proton signals observed at δ 11.3 ppm in the spectrum of the free ligand was found to be absent, confirming the subsequent involvement of deprotonated hydroxyls in chelation to the metal ions [38]. The broad signal appeared at δ 4.9 ppm, was not found in the spectrum of the free ligand due to the resonance of protons of coordinated water molecules [disappeared after addition of D_2O due to proton exchange] [21]. The ^{13}C NMR spectrum of zinc complex showed chemical shift to higher value at 146.9 ppm (C6-ipso) and 130.2 ppm (C1-ipso) in comparison with the signal of free ligand suggest that coordination through nitrogen of azomethine (C=N) and oxygen of oxime (C=N–OH) group. No changes in signals of other carbon atoms are detected.

3.2.4 Electron Spin Resonance (ESR) Spectra

The electron spin resonance (ESR) spectrum of Cu(II) complex **4**; Fig. 5 in solid state gives axial signal shape and have symmetric bands with two *g* values, $g_{\|} = 2.28$, $g_{\perp} = 2.04$. These values suggest a tetrahedral stereochemistry for the complex. The average g value equals 2.12 was

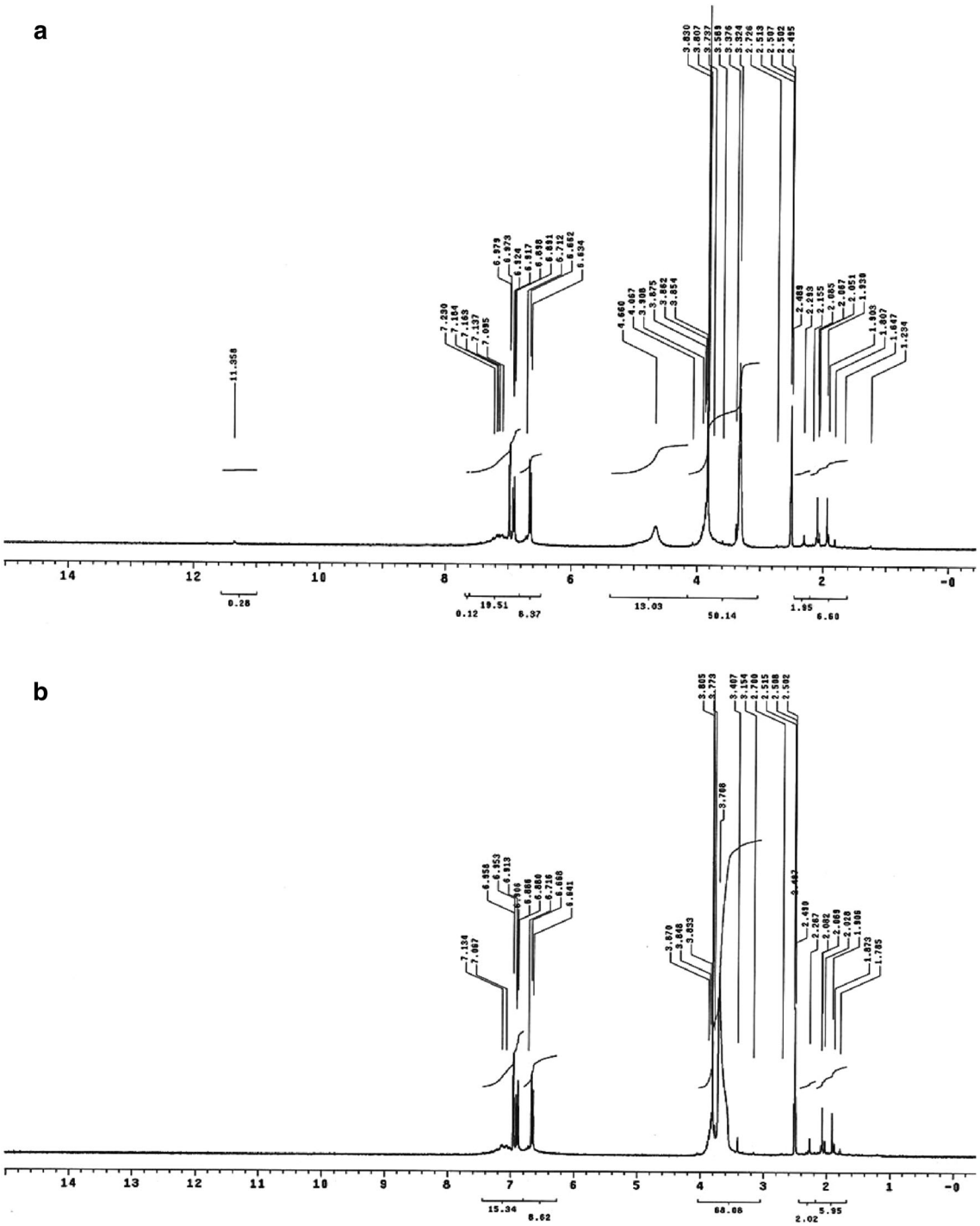

Fig. 2 **a** The ^{1}HNMR Spectrum of $\mathbf{H_2L}$ in (DMSO). **b** The ^{1}HNMR Spectrum of $\mathbf{H_2L}$ in (DMSO + D_2O)

calculated according to the equation $g_{av} = 1/3[g_{\|} + 2g_{\perp}]$. Complex **4** exhibits $g_{\|} < 2.3$, suggesting covalent characters of the copper-ligand bonding in this complex [39]. From the observed trend $g_{\|} > g_{\perp} > 2.0023$, it is clear that the unpaired electron lies predominantly in $d_{x^2-y^2}$ orbital, giving $2B_{1g}$ as the ground state [40]. The exchange interaction (axial) parameter (G), calculated as $G = (g_{\|} - 2.0023)/(g_{\perp} - 2.0023)$, and found for the present copper(II) complex as 7.3, suggests that the local tetragonal axes are aligned parallel and the exchange interactions between copper(II) centers in the solid state are negligible [41, 42]. The ESR spectral parameter of Cu(II) in complex has tetra hedral geometry around Cu(II) ions. These data are well consistent with other reported values [43].

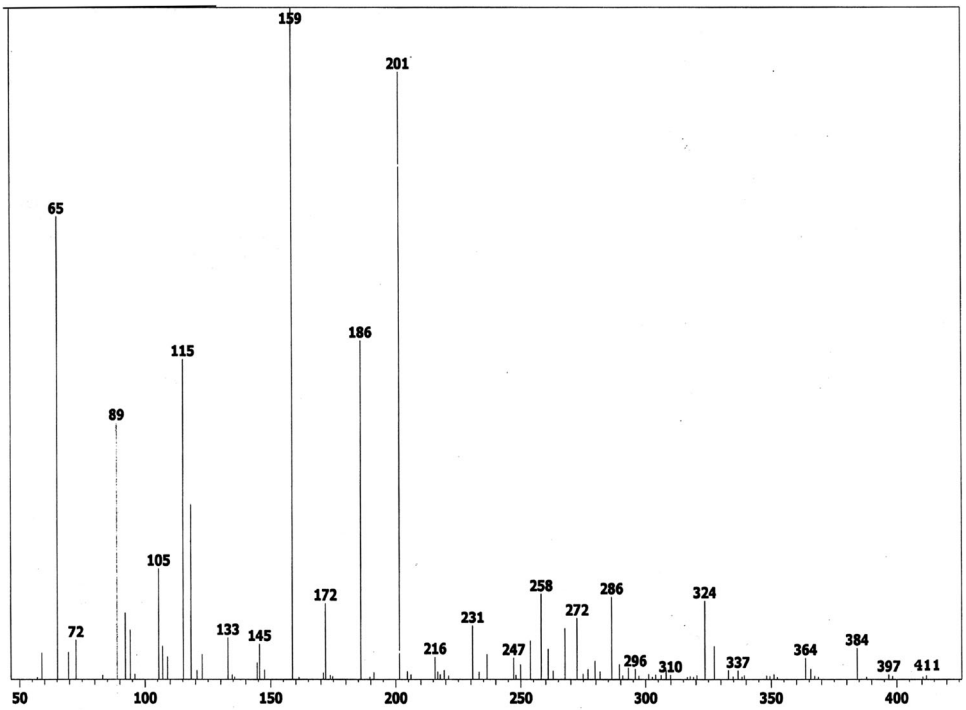

Fig. 3 The mass spectrum of H_2L

3.2.5 Thermal Studies

The thermo gravimetric analysis (TGA) curves for complexes were obtained at a heating rate of 10 °C/min and flowing nitrogen atmosphere over a temperature range of room temperature 800 °C and the proposed decomposition data were recorded in Table 2. As examples, Figs. 6 and 7 show the thermograms obtained for complexes **2** and **3**.

The first step with small mass losses occurs between 80 and 90 °C, due to loss of outer sphere crystalline water. The removal of coordinated water molecules appeared at higher temperature (>110–120 °C). The complexes show multi-step decomposition due to thermal degradation of organic part of ligands. The final weight loss matches with the formation of metal oxides as the stable end product.

From the thermogravimetric analysis, the overall weight losses for **2**, **3**, **4,** and **5** complexes agree well with the proposed formula obtained by elemental analysis, IR, ^{1}H, ^{13}C NMR, mass, ESR, and magnetic susceptibility measurements. The proposed structures as in Fig. 8 have been assigned for the metal complexes.

3.3 Corrosion Inhibition Studies

3.3.1 Weight Loss Technique

The corrosion rate (CR) in mils per year (MPY) and percentage corrosion inhibition efficiency (IE% $= \mu_w\%$) were calculated using the Eqs. (1) and (2), respectively [44].

$$\mathrm{CR} = W \cdot 534/A \cdot d \cdot t, \tag{1}$$

where $W =$ weight loss (g), $d =$ density of mild steel (7.85 g/cm^3), $A =$ area of specimen (sq.cm), $T =$ exposure time (h).

$$\mu_w\% = \left((C_R^0 - C_R^i)/C_R^0\right) \times 100, \tag{2}$$

where C_R^0 and C_R^i are the corrosion rates in absence and presence of inhibitors, respectively.

From the evaluated weight loss, surface coverage (θ) was calculated using Eq. (3):

$$\theta = \left(C_R^0 - C_R^i/C_R^0\right) \tag{3}$$

The values of percentage inhibition efficiency ($\mu_{WL}\%$), corrosion rate (CR), and surface coverage (θ) obtained from weight loss method at different concentrations of all compounds at 293 K are summarized in Table 3.

From the data, the Schiff base and its complexes show appreciable corrosion inhibition for carbon steel in 0.5 M HCl medium. The effect of inhibitor concentration on inhibition efficiency in the presence of different concentrations of the Schiff base and its complexes show that the maximum inhibition efficiency is at 7×10^{-4} Mol/dm^3 in 0.5 M HCl solution. The Co(II) complex **2** exhibited the greatest impact on corrosion inhibition among the other compounds as they appear in the chart (1). It was found that the efficiency order followed by compounds is **2** > **3** > **5** > **1** > **4**.

In order to get good reproducibility, experiments were carried out from two to three times per test. In the present

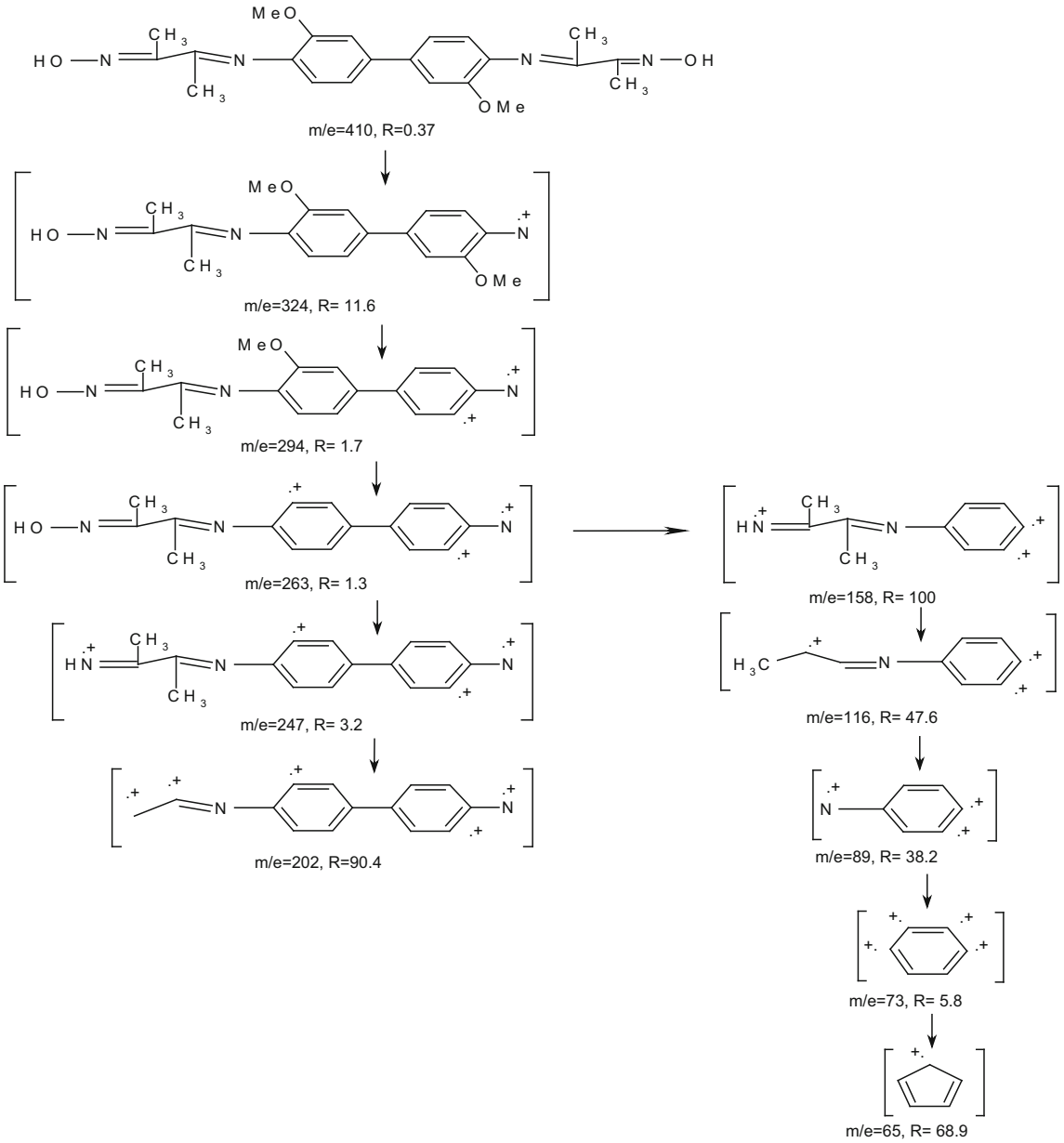

Scheme 1 The mass fragmentation pattern of Schiff base ligand $\mathbf{H_2L^1}$

Table 1 IR spectral data for compounds **1–5**

Comp	H_2O	OH	CH ar	CH aliph	C=N	ν(N–O) oxime	M–O	M–N	M–Cl
1	–	3441	3090	2860	1620	1030	–	–	–
2	3385	–	3022	2954	1608	1061	615	584	312
3	3377	–	3035	2934	1608	1060	660	615	316
4	3425	–	2920	2850	1598	1059	660	584	315
5	3488	–	3075	2925	1610	1063	660	589	318

study, the standard deviation values among parallel test experiments were found to be smaller than 4 %, indicating good reproducibility. Also, we calculated some statistical analysis (Table 4) as mean, median, mode, standard deviation, minimum, and maximum values for each group to measure inhibition efficiency of compounds to corrosion of metals. From Table 4, we can obtain the minimum and maximum inhibition efficiencies of the compounds. The

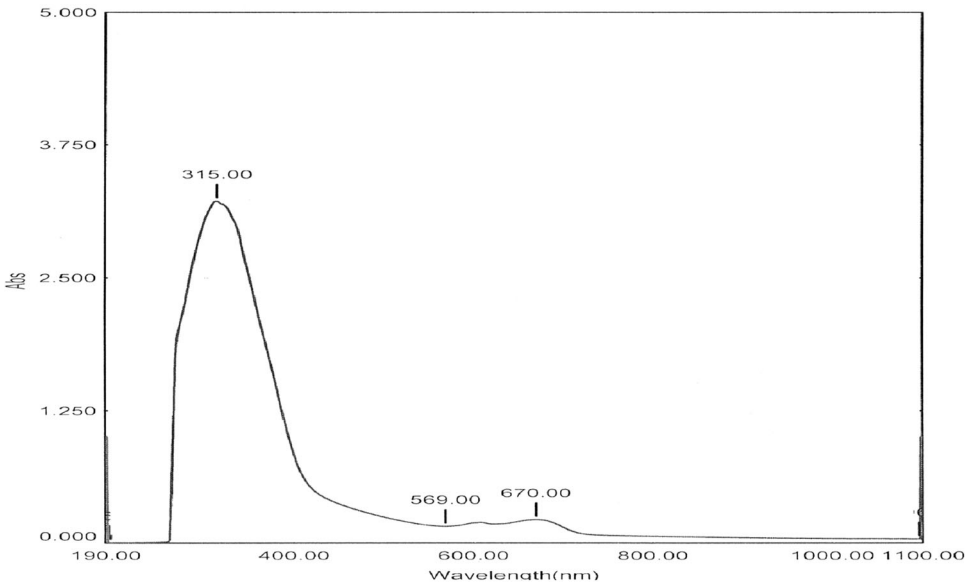

Fig. 4 Electronic spectrum of complex **2**

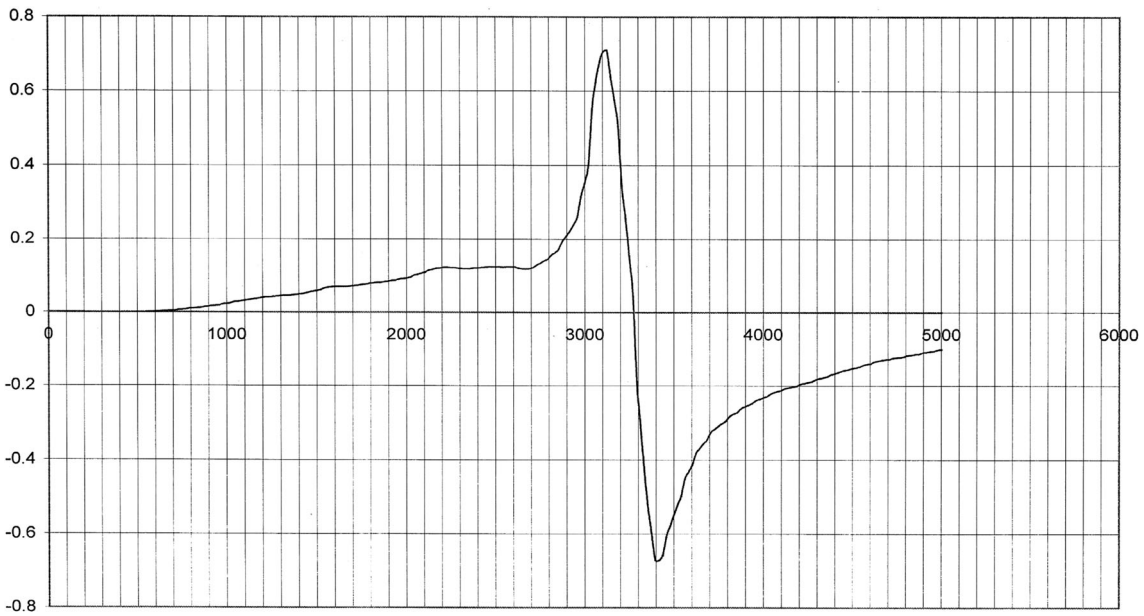

Fig. 5 ESR spectrum of Cu(II) complex **4**

order of inhibition efficiency of compounds is the following: **2** > **3** > **5** > **1** > **4**.

3.3.2 Potentiodynamic Polarization

The linear Tafel segments of anodic and cathodic curves were extrapolated to the corrosion potential to obtain corrosion current densities (i_{corr}). From the polarization curves obtained, Figs. 9a–e, the corrosion current (i_{corr}) was calculated by curve fitting using the Eqs. (4) and (5):

$$I = i_{corr}\left[\exp\left(\frac{2.3\Delta E}{b_a}\right) - \exp\left(-\frac{2.3\Delta E}{b_c}\right)\right] \quad (4)$$

The inhibition efficiency was evaluated from the measured i_{corr} values using the relationship:

$$\mu_p\% = \frac{i^0_{corr} - i^i_{corr}}{i^0_{corr}} \times 100, \quad (5)$$

where i^0_{corr} and i^i_{corr} are the corrosion current densities in the absence and presence of inhibitors, respectively. The electrochemical polarization parameters of steel corrosion

Table 2 Thermal gravimetric analysis for compounds **2**, **3**, **4**, and **5**

Compound no.	Stages	Temp. range (°C)	Calculated %	Found %	Percent error %	Assignment
2	First step	20–110	15.90	15.30	3.9	2 Crystalline $H_2O + Cl_2$
	Second step	110–403	21.70	21.30	1.9	2 Coordinated $H_2O + 2C_4H_7$
	Third step	403–503	13.70	12.80	7	$2NO_2$
	Fourth step	503–652	26.00	23.50	10	Decomposition of organic part of ligand $(2C_7H_6) + N_2 + O_2$
	Residue	652–800	16.10	15.60	3.2	1.45 CoO
3	First step	20–120	12.30	13.20	−6.8	2 Crystalline $H_2O + NO_2$
	Second and Third step	120–482	28.60	28.10	1.8	2 Coordinated $H_2O + NO_2 + 2C_4H_7$
	Fourth step	482–660	37.50	38.90	−3.6	Decomposition of Organic part of ligand $(2C_7H_6) + Cl_2$
	Residue	660–800	20.00	19.60	2.0	1.8 NiO
4	First step	20–123	5.30	5.30	0.0	2 Crystalline H_2O
	Second step	123–242	9.40	10.70	−12.0	2 Coordinated $H_2O + N_2$
	Third step	242–374	26.60	27.70	−3.9	Decomposition of organic part of ligand $(2C_4H_7) + Cl_2$
	Fourth step	374–623	40.00	43.00	−6.9	Decomposition of organic part of ligand $(2C_7H_6) + 2NO_2$
	Residue	623–800	14.00	13.00	7.6	1.25 CuO
5	First step	20–130	13.00	12.40	4.8	1 Crystalline $H_2O + Cl_2$
	Second step	130–300	7.90	8.90	−11.2	1 Crystalline H_2O + 2 Coordinated $H_2O + N_2$
	Third step	300–497	13.4	13.5	−0.7	$2NO_2$
	Fourth step	497–695	51.20	54.00	−5.2	Decomposition of Organic part of ligand $(2C_7H_6)$ & $(2C_4H_7) + NO$
	Residue	695–800	13.00	12.00	4.8	1.1 ZnO

in 0.5 M HCl in the presence and absence of various concentrations of Schiff base and its complexes and the corresponding corrosion efficiencies using Nova 1.10 program are given in Table 5.

The obtained results show that the inhibition efficiencies increase in the case of all used compounds when the inhibitor concentration increases. The efficiency order is as **2** > **3** > **5** > **1** > **4**.

The results obtained from the polarization measurements are in good agreement with those obtained from the weight loss method and render to it. Also, addition of studied compounds effected both anodic and cathodic reactions. Therefore, those compounds could be classified as mixed type (anodic/cathodic) inhibitors.

3.3.3 Adsorption Isotherm

The increase in the inhibition efficiency of carbon steel in 0.5 M HCl solution, with increasing compound concentration can be explained on the basis of additive adsorption. In the present medium, the additives were shown the linear plots for C/θ versus Conc. and are suggested to obey the Langmuir adsorption isotherm as seen in Fig. 10, according to the following Eq. (6):

$$\theta/(1-\theta) = KC, \tag{6}$$

where θ is the surface coverage, C is concentration of inhibitors, and K is the adsorption equilibrium constant which also represents the degree of adsorption (i.e., the higher value of K indicate that inhibitor is strongly adsorbed on the metal surface); the K obtained from the reciprocal of the intercept of Langmuir plot lines and the slope of these lines is near unity, meaning that each inhibitor molecule occupies one active site on the metal surface.

3.3.4 Scanning Optical Microscope

The optical images of carbon steel sample Fig. 11a shows degradation of carbon steel in the absence of inhibitors. The degradation appears more at grain boundary, since these regions are most susceptible to corrosion, and may be responsible for the high rate of corrosion. The optical images Figs. 11b–f of the carbon steel after corrosion in acid medium containing inhibitors show adsorbed layer of

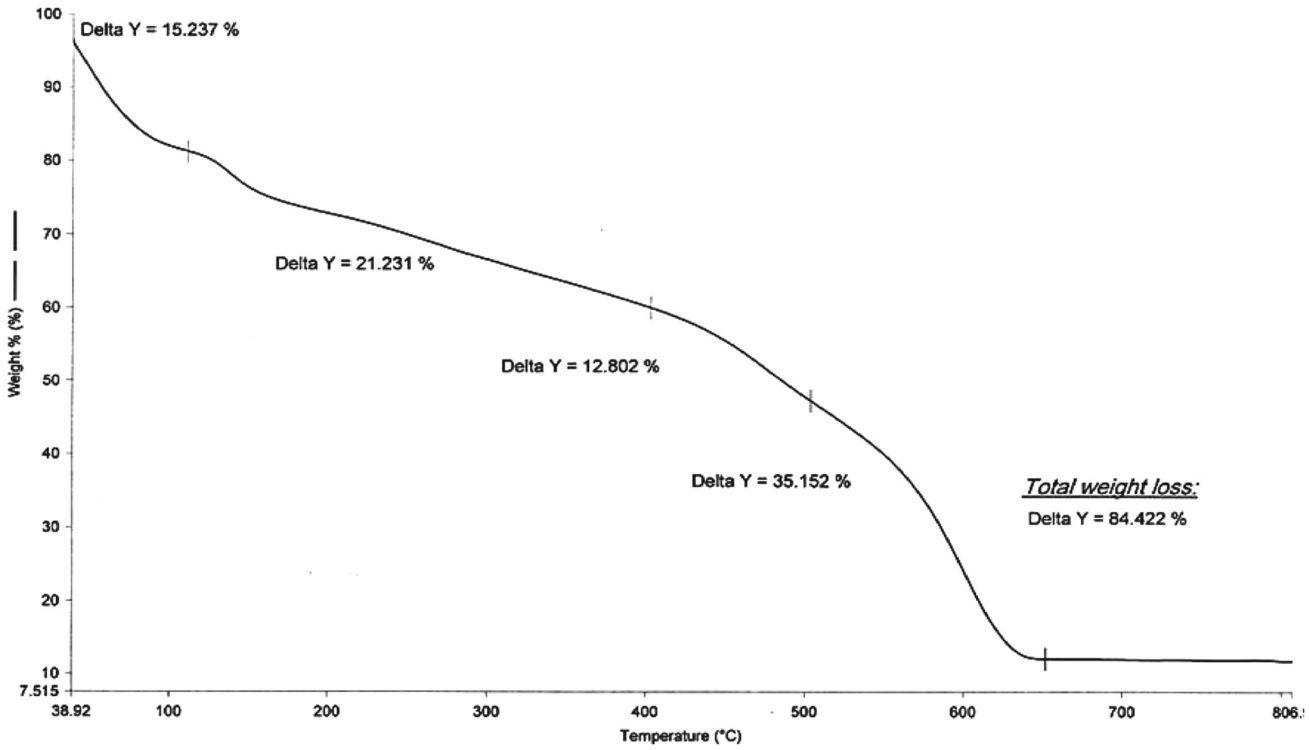

Fig. 6 TGA of complex **2**

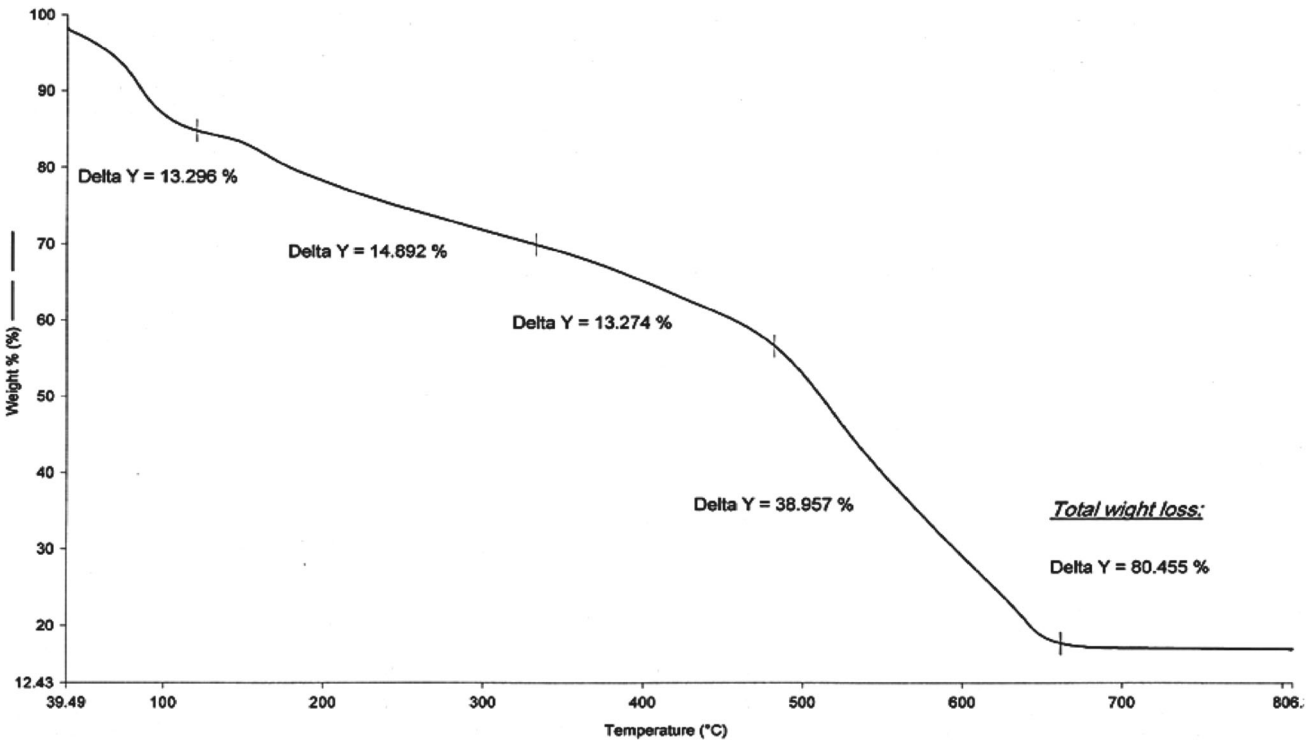

Fig. 7 TGA of complex **3**

inhibitor molecules on the metal surface, thus protecting the metal.

3.3.5 Mechanism of Corrosion Inhibition

The TGA results show that the compounds can be used as corrosion inhibitors under conditions that do not surpass 90 °C which is the onset temperature of the complexes

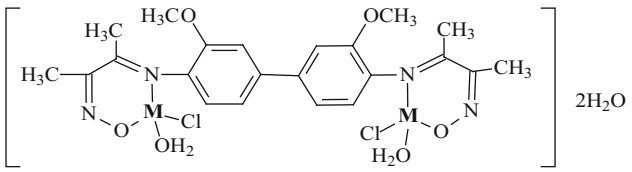

M= Co, Ni, Cu and Zn

Fig. 8 The proposed structure of complexes **2**–**5**

degradation. Increasing of temperature may lead to partial decomposition of the complexes. Also, it was reported that, the increasing of temperature caused the partial decomposition of the coating film and separated from carbon steel surface [45].

It can be seen from the data that the Schiff base (H_2L,1) and its complexes exhibited good corrosion inhibition against corrosion of mild steel in acidic medium which may be attributed to the presence of π electrons in aromatic systems and multiple bonds, presence of azomethine group, and the electronegative atoms (O and N) In the inhibitor molecules structures [46]. The effect of additional methoxy substituent groups on the aromatic ring. The methoxy group exhibits an inductive effect that results in the increase of the electron density and the activation of the aromatic ring, which may impact better absorptivity to the inhibitor which improve adsorption and protection. This suggests that corrosion inhibition is a result of adsorption

Table 3 The corrosion rate, surface coverage, and inhibition efficiency values for the corrosion of mild steel in aqueous solution of 0.5 M HCl in the absence and in the presence of different concentrations of different inhibitors from weight loss measurements

Compound	Concentration (M)	CR (mm/year)	θ	IE%
Blank	0.5 M HCl	0.0035	–	–
1	0.0001	0.000874011	0.728374	72.83737
	0.0003	0.000768239	0.761246	76.12457
	0.0005	0.000462057	0.856401	85.64014
	0.0007	0.000395254	0.877163	87.71626
2	0.0001	0.000740405	0.769896	76.98962
	0.0003	0.000718137	0.776817	77.68166
	0.0005	0.000292265	0.90917	90.91696
	0.0007	0.000208761	0.935121	93.51211
3	0.0001	0.000896279	0.721453	72.14533
	0.0003	0.00064855	0.798443	79.84429
	0.0005	0.000489892	0.847751	84.77509
	0.0007	0.000211544	0.934256	93.42561
4	0.0001	0.00099116	0.688581	68.85813
	0.0003	0.000613968	0.807093	80.70934
	0.0005	0.00058093	0.817474	81.7474
	0.0007	0.000528618	0.83391	83.391
5	0.0001	0.000578176	0.818339	81.83391
	0.0003	0.000481814	0.848616	84.86159
	0.0005	0.000371685	0.883218	88.3218
	0.0007	0.000294595	0.907439	90.74394

Table 4 Some statistical analysis for **1**, **2**, **3**, **4**, and **5** compounds for studying the inhibition efficiency of corrosion of metal in acid medium by weight loss method

Compound	Mean	Median	Mode	SD	Minimum value	Maximum value
1	80.6	80.8	72.8, 76.1, 85.6, 87.7	7.2	72.8	87.7
2	84.7	84.3	76.9, 77.6, 90.9, 93.5	8.6	76.9	93.5
3	82.5	82.3	72.1, 79.8, 84.7, 93.4	8.9	72.1	93.4
4	78.6	81.2	68.8, 80.7, 81.7, 83.3	6.6	68.8	83.3
5	86.4	86.5	81.8, 84.8, 88.3, 90.7	3.9	81.8	90.7
All compounds	82.6	82.6	–	7.1	68.8	93.5

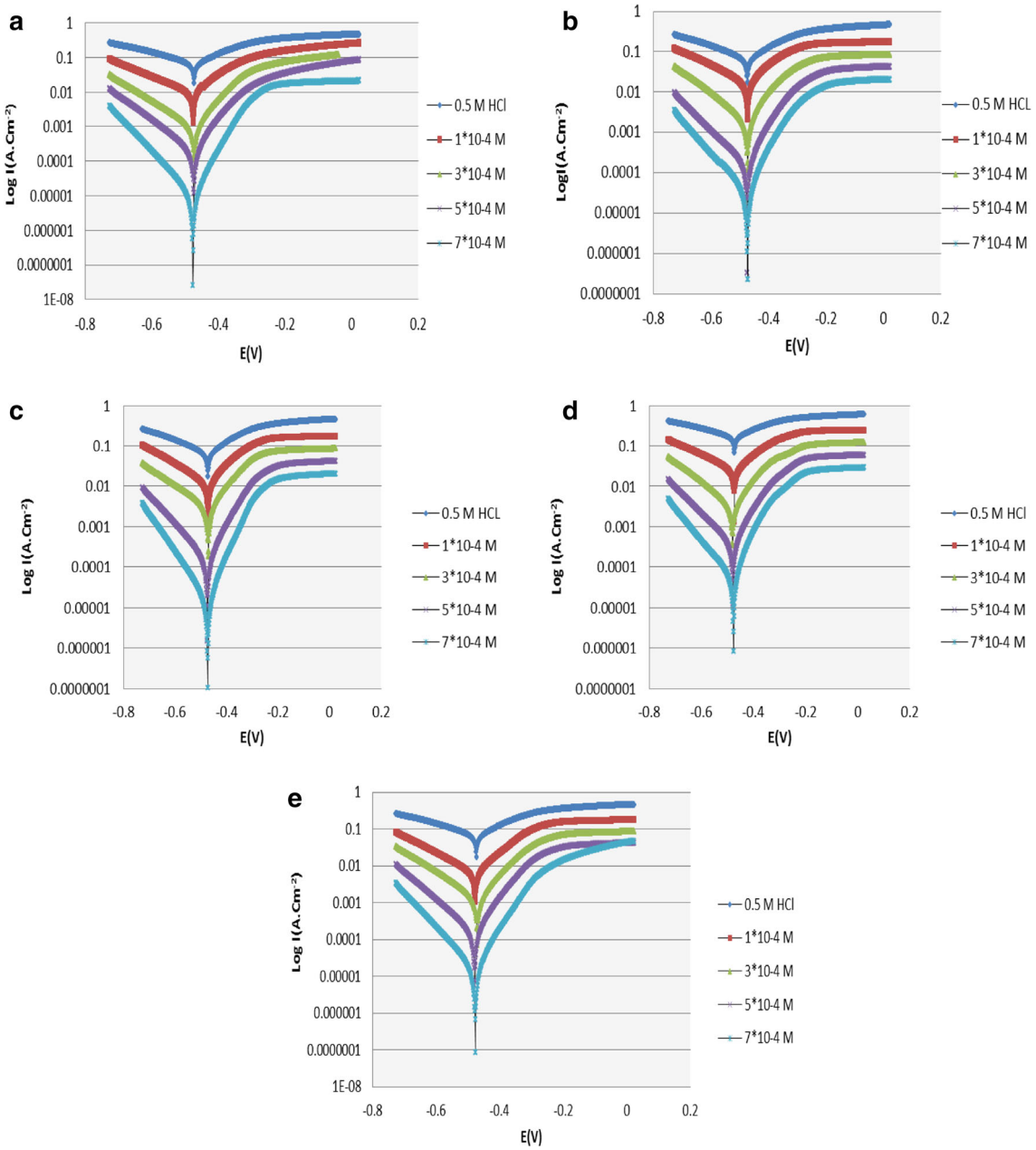

Fig. 9 Polarization curves for mild steel in the presence of different concentrations of compounds **1** (**a**), **2** (**b**), **3** (**c**), **4** (**d**), and **5** (**e**)

of inhibitors on the metal surface and the compounds act as adsorption inhibitors. Also, it should be emphasized that, the large size and high molecular weight of the compounds can contribute to the greater inhibition efficiency.

3.4 Antibacterial Activity

Sulfate-reducing bacteria (SRB) are commonly considered the main culprits of microbially influenced corrosion (MIC) due to their characteristic corrosion product iron sulfide which are ubiquitously associated with anaerobic corrosion damage. The results of antibacterial activity of Schiff base ligand $\mathbf{H_2L}$ and its complexes against (SRB)-stabilized mixed culture are clear in Fig. 12. The antibacterial activity tests were carried out in four concentrations 100, 300, 500, and 700 ppm and showed a good antibacterial activity. The most active compound comparison with other is **4** which is followed by **2** and **5**. From the results, the antibacterial activity was increased with the increasing concentration of compounds and the lowest concentration of **4** with a good antimicrobial activity is 300 ppm. The results revealed that the SRB activity was less inhibited using compound **1**. The antibacterial activity of compounds due to the interaction of biocides with surface cell causes

Table 5 Polarization parameters of Schiff base H_2L and its complexes

Comps.	Conc.	b_a	b_c	$E_{corr.}$	$I_{corr.}$	CR	IE%
1	Blank	47.6	71.3	−478.3	119.34	0.9236	–
	1×10^{-4}	48.6	56.5	−490.0	19.54	0.1175	83.6
	3×10^{-4}	32.0	32.9	−492.9	16	0.1129	86.5
	5×10^{-4}	16.3	14.2	−493.6	13.9	0.802	88.6
	7×10^{-4}	18.46	14.6	−481.6	11.34	0.1079	90.5
2	Blank	55.8	71.9	−479.0	246.8	1.90	–
	1×10^{-4}	24.4	19.9	−495.3	43.2	0.3349	82.4
	3×10^{-4}	35.9	42.7	−494.1	39.7	0.3082	83.8
	5×10^{-4}	42.7	59.2	−440.2	27.4	0.3179	88.8
	7×10^{-4}	35.3	35.7	−442.5	21.0	0.1965	91.4
3	Blank	47.6	71.3	−478.3	119.34	0.9236	–
	1×10^{-4}	21.8	17.4	−463.9	25.6	0.1577	78.5
	3×10^{-4}	13.44	17.03	−446.6	20.6	0.1985	82.7
	5×10^{-4}	22.9	13.6	−450.6	10.6	0.8	91.1
	7×10^{-4}	19.5	16.6	−452	6.8	0.05	94.3
4	Blank	47.6	71.3	−478.3	119.34	0.9236	–
	1×10^{-4}	40.5	32.6	−472.9	27.6	0.2140	76.8
	3×10^{-4}	37.4	47.6	−464.5	24.8	0.1866	79.8
	5×10^{-4}	44.7	48.9	−459.0	21.14	0.1638	82.2
	7×10^{-4}	34.04	38.6	−453.4	19.4	0.1476	84.0
5	Blank	47.6	71.3	−478.3	119.3	0.9236	–
	1×10^{-4}	57.6	90.4	−458.2	27.6	0.2142	76.8
	3×10^{-4}	40.9	47.2	−468.7	26.33	0.2040	77.9
	5×10^{-4}	30.46	29.90	−463.3	15.45	0.1197	87.5
	7×10^{-4}	30.27	30.30	−453.3	11.37	0.0881	90.4

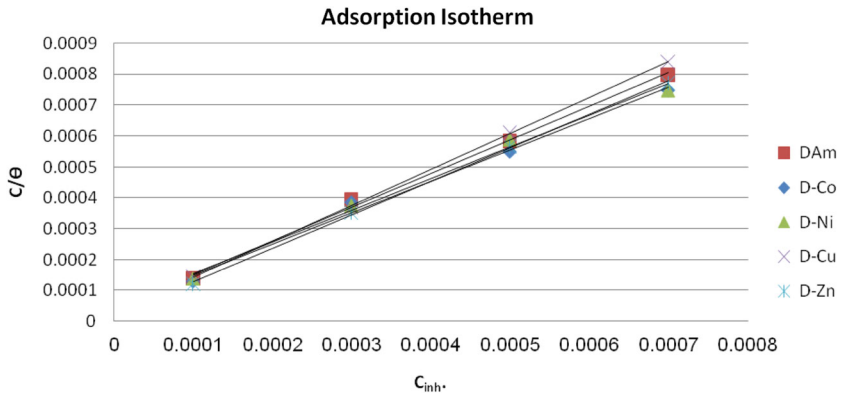

Fig. 10 Langmuir isotherm of H_2L and its complexes at 20 °C on carbon steel surface

destruction of the microstructure of the cell wall and the cytoplasmic membrane [47, 48].

3.4.1 Mechanism of Antimicrobial Activity

Schiff bases having chelation with oxygen, nitrogen donors, and their complexes have been used as drugs and possess a wide variety of biological activities against bacteria, fungi, and certain types of tumors and also, they have many biochemical, clinical, and pharmacological properties due to the presence of azomethine group (–N=CH–) which imports in elucidating the mechanism of transformation and racemization reaction biologically. In general in this work, the metal chelates show higher antimicrobial activity than the parent Schiff base. The good antimicrobial activity of metal complexes than Schiff base ligand is due to chelation theory [49], which suggests that the chelation process increases the delocalization of the π-electrons over the whole chelate ring, which results in an increase in the lipophilicity of the metal complexes.

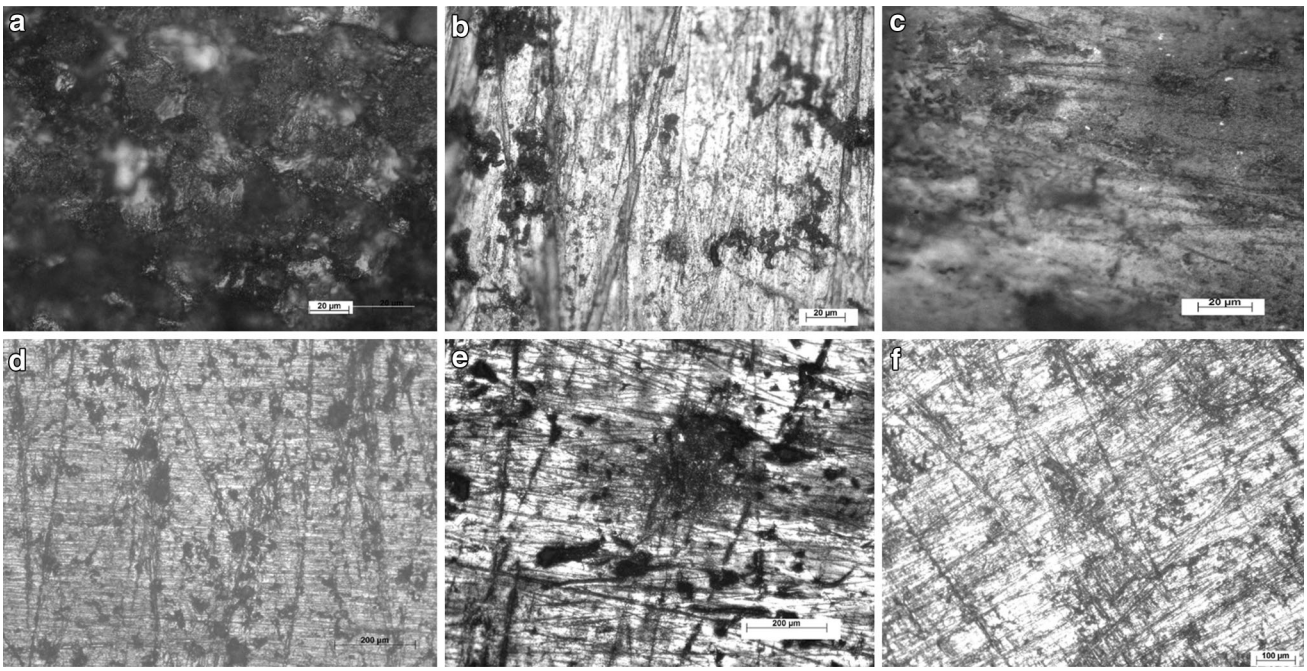

Fig. 11 Optical microscope images of carbon steel sample in acid medium without inhibitor (**a**), and with inhibitors $\mathbf{H_2L^1}$ (**b**), **2** (**c**), **3** (**d**), **4** (**e**), and **5** (**f**)

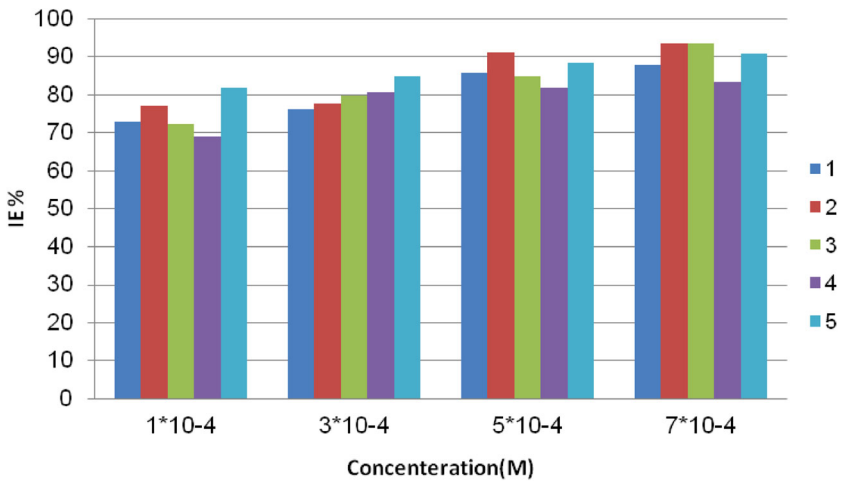

Fig. 12 The inhibition efficiency of different concentrations from Schiff base (**1**) and its complexes (**2**–**5**) in 0.5 M HCl solution

Consequently, the metal complexes can easily penetrate into the lipid membranes and block the metal binding sites of enzymes of the microorganisms. These metal complexes also affect the respiration process of the cell and thus block the synthesis of proteins, which restricts further growth of the organism.

4 Conclusion

New homobimetallic complexes with Schiff base Bis(diacetylmonoxime)biphenyl-3,3′-dimethoxy-4,4′-diamine were prepared and investigated. The structure of the ligand and its complexes were determined by elemental analysis, magnetic moment, and mass, UV, IR, ^{1}H NMR, ^{13}C spectra. The Schiff base and its complexes were tested as corrosion inhibitors and fined as mixed type inhibitors as evident from the weight loss and potentiodynamic polarization techniques. The inhibitor efficiencies of compounds increase with increasing concentration of the compounds. The order of inhibition efficiency follows the following pattern **2** > **3** > **5**>**1** > **4**, due to increasing of the molecular weight of compounds. The inhibitors obey Langmuir adsorption isotherm. Also, the optical microscope images revealed protection of metal surface in the HCl medium by the adsorption of inhibitors on the surface of the metal. The

synthesized compounds appeared a good antibacterial activity against SRB which can cause corrosion. Finally, the synthesized compounds can be used in double purpose as corrosion inhibitors and as biocides.

Acknowledgments The authors are thankful to Dr. Ahmed Ismail in CMRDI for his assistance in taking optical microscope images. Also, we thankful Dr. Musttfa Abo El Soud in National Research Center for his assistance in antibacterial activity analysis.

References

1. Sun W, Nesic S (2007) A mechanistic model of H_2S corrosion of mild steel, NACE International corrosion conference & Expo. Houston, Texas, USA, paper No. 07655, (2007)1–26.
2. Tao Z, Zhang S, Li W, Hou B (2009) Corrosion inhibition of mild steel in acidic solution by some oxo-triazole derivatives. Corros Sci 51:2588–2595
3. Trabanelli G (1991) Inhibitors-an old remedy for a new challenge. Corrosion 47:410–419
4. Raman A, Labine P (1986) Reviews on Corrosion Inhibitor Science and Technology, vol 1. NACE, Houston, p 5
5. Hosseini MG, Mertens SFL, Ghorbani M, Arshadi MR (2003) Asymmetrical Schiff bases as inhibitors of mild steel corrosion in sulfuric acid media. Mater Chem Phys 78:800–808
6. Singh AK, Quraishi MA (2010) Effect of Cefazolin on the corrosion of mild steel in HCl solution. Corros Sci 52:152–160
7. Singh AK, Quraishi MA, Ebenso EE (2011) Inhibitive effect of cefuroxime on the corrosion of mild steel in hydrochloric acid solution. Int J Electrochem Sci 6:5673–5688
8. Singh AK, Quraishi MA (2012) Study of some bidentate schiff bases of isatin as corrosion inhibitors for mild steel in hydrochloric acid solution. Int J Electrochem Sci 7:3222–3241
9. Shokry H, Yuasa M, Sekine I, Issa RM, El Baradie HY, Gomma GK (1998) Corrosion inhibition of mild steel by schiff base compounds in various aqueous solutions. Corros Sci 40: 2173–2186
10. Emregül KC, Atakol O (2003) Corrosion inhibition of mild steel with schiff base compounds in 1 M HCl. Mater Chem Phys 82:188–193
11. Kumar A (2013) Corrosion resistance properties of benzhydrylidene-(3, 5-dimethoxy-phenyl)-amine on mild steel in 0. 5M sulphuric acid media. Int J Chem Appl 5:191–197
12. Emregül KC, Kurtaran R, Atakol O (2003) An investigation of chloride-substituted Schiff bases as corrosion inhibitors for steel. Corros Sci 45:2803–2817
13. Li S, Chen S, Lei S, Ma H, Yu R, Liu D (1999) Investigation on some Schiff bases as HCl corrosion inhibitors for copper. Corros Sci 41:1273–1287
14. Agrawal YK, Talati JD, Shah MD, Desai MN, Shah NK (2004) Schiff bases of ethylenediamine as corrosion inhibitors of zinc in sulphuric acid. Corros Sci 46:633–651
15. Mahdavian M, Attar MM (2009) Electrochemical behaviour of some transition metal acetylacetonate complexes as corrosion inhibitors for mild steel. Corros Sci 51:409–414
16. Poornima T, Nayak J, Shetty AN (2012) Effect of diacetyl monoxime thiosemicarbazone on the corrosion of aged 18 Ni 250 grade maraging steel in sulphuric acid solution. J Metall 2012: 1–13
17. Hamilton WA (1985) Sulphate-reducing bacteria and anaerobic corrosion. Annu Rev Microbiol 39:195–217
18. Javaherdashti R, Raman SRK, Panter C, Pereloma EV (2006) Microbiologically assisted stress corrosion cracking of carbon steel in mixed and pure cultures of sulfate reducing bacteria. Biodegradation 58:27–35
19. Azzam EMS, Sami RM, Kandile NG (2012) Activity inhibition of sulfate reducing bacteria using some cationic thiol surfactants and their nanostructures. Am J Biochem 2:29–35
20. Vester F, Ingvorsen K (1998) Improved most-probable-number method to detect sulfate-reducing bacteria with natural media and a radiotracer. Appl Environ Microbiol 64(5):1700–1707
21. Nassar AM, Hassan AM, Ibraheem NM, Hekal BH (2015) Synthesis and comparative studies of cyclopalladated complexes With ortho C-H activation of aromatic rings bearing electron donating and electron withdrawing groups. Synth React Inorg Met Org Nano Met Chem 45:813–820
22. Nonyama M, Tomita S, Yamasaki K (1975) N(2-pyridyle)acetamide complexes of metal ions. Inorg. Chim Acta 12:33–37
23. Bullock JI, Tajmir-Riahi HA (1978) Schiff-base complexes of the lanthanoids and actinoids. Part 1. Lanthanoid(III) halide complexes with the un-ionised form of NN′-ethyl-enebis(salicylideneimine) and related bases. J Chem Soc Dalton Trans 1:36–39
24. Rakha TH (1999) Mononuclear and binuclear chelates of biacetylmonoxime picolinoylhydrazone. Trans Met Chem 24: 659–665
25. Teixeira LHP, Fraga CAM, Barreiro EJ (1998) Synthesis of new 1,2-benzothiazin-3-one derivatives, designed as dual cyclooxigenase and 5-lipooxigenase inhibitors candidates. J Braz Chem Soc 9:119–130
26. Lin-Vien D, Clothup NB, Fateley WG, Grasselli JG (1991) The hand book of infrared and Raman chracteristic frequencieis of organic molecules. Academic Press, San Diego
27. Nassar AM, Hassan AM, Al-Abd SS (2015) Antitumor and antimicrobial activities of novel palladacycles with abnormal aliphatic C-H activation of Schiff Base 2-[(3-phenylallylidene)amino] phenol. Synth React Inorg Met Org Nano Met Chem 45:256–270
28. Mobinikhaledi A, Forughifar N, Kalhor M (2010) An efficient synthesis of Schiff bases containing benzimidazole moiety catalyzed by transition metal nitrates. Turk J Chem 34:367–373
29. Anupama B, Kumari CG (2013) Cobalt (II) complexes of ONO donor Schiff bases and N, N donor ligands: synthesis, characterization, antimicrobial and DNA binding study. Int J Res Chem Environ 3:172–180
30. Ummathur MB, Sayudevi P, Krishnankutty K (2009) Schiff bases of 3-[2-(1,3-benzothiazol-2-yl)hydrazinylidene] pentane-2,4-dione with aliphatic diamines and their metal complexes. J Arg Chem Soc 97:31–39
31. Karvembu R, Hemalatha S, Prabhakaran R, Natarajan K (2003) Synthesis, characterization and catalytic activities of ruthenium complexes containing triphenylphosphine/triphenylarsine and tetradentate Schiff bases. Inorg Chem Commun 6:486–490
32. Aliyu HN, Mohammed AS (2009) Synthesis and characterization of Iron (II) and Nickel (II) Schiff base complexes. Bajopas 2:132–134
33. Krushnalal TJ, Pancholi AM, Pandaya KS, Thakar AS (2011) Synthesis, characterization and antibacterial activity of novel schiff base derived from 4-acetyl-3-methyl-1-(4'-methyl- phenyl)-2-pyrazolin-5-one and its transition metal complexes. J Res Chem Environ 1:63–69
34. Budagumpia S, Shetti UN, Kulkarnia NV, Revankara VK (2009) Ligational behaviour of bidentate coumarin derivative towards Co(II), Ni(II) and Cu(II) synthesis, characterization, electrochemistry and antimicrobial studies. J Coord Chem 62: 3961–3968
35. Spinu C, Kriza A (2000) Co(II), Ni(II), and Cu(II) complexes of bidentate Schiff bases. Acta Chim Slov 47:179–185
36. Raman N, Raja YP, Kulandaisamy A (2001) Synthesis and characterisation of Cu(II), Ni(II), Mn(II), Zn(II(, and VO(II)

Schiff base complexes derived from o-phenylenediamine and acetoacetanilide. Indian Acad Sci 113(2001):183–189
37. Rehman S, Ikram M, Islam N, Jan N (2011) Synthesis and characterization of Ni(II), Cu(II) and Zn(II) tetrahedral transition metal complexes of modified hydrazine. J Mex Chem Soc 55: 164–167
38. Liang YM, Liu CM, Ma YX (1998) formyl ferrocene 5-phenyloxazole-2-carbonylhydrazone bivalent transition-metal complexes. Trans Met Chem 23:97–99
39. Lever ABP (1984) Inorganic electronic spectroscopy, 2nd edn. Elsevier, New York
40. Speir G, Csihony J, Whalen AM, Pierpont CG (1996) Studies on aerobic reactions of ammonia/3,5-Di-*tert*-butylcatechol Schiff-base condensation products with Cu, Cu(I), and Cu(II). Strong Cu(II)-radical ferromagnetic exchange and observations on a unique N-N coupling reaction. Inorg Chem 35:3519–3524
41. Hathaway BJ, Bardley JN, Gillard RD (1971) Essays in chemistry. Academic Press, New York
42. Hathway BJ (1984) Structure and Bonding. Springer, Berlin 57:55–118
43. Jeyasubramanian K, Thambidurai S, Ramalingam S, Murugesan R (1998) Spectral and redox models for blue copper proteins: copper(II) complexes of β-diketonimines from a Knoevenagel condensate. J Inorg Biochem 72:101–107
44. Narayan R (1983) An introduction to metallic corrosion and its prevention, 1st edn. Oxford and IBH, Oxford
45. Bahkahk CK, Hadi JS (2015) New unsymmetrical Schiff base as inhibitor of carbon steel corrosion and antibacterial activity. Res J Chem Sci 5(1):64–70
46. Singh AK, Quraishi MA (2012) Study of some bidentate schiff bases of isatin as corrosion inhibitors for mild steel in hydrochloric acid solution. Int J Electrochim Sci 7:3222–3241
47. American Public Health Association (APHA) (1989) Stander methods for the examination of water and waste water, 17th edn. APHA, New York
48. Ghazy EA, Eweas AF (2006) Microbial corrosion of mild steel and its inhibition. Chem A 3:321–327
49. Jejurkar CR, Parikh K (1997) Synthesis and characterization of Schiff base complexes of Copper(II), Nickel(II), Vanduim(IV), and Uranium(VI). Asian J Chem 9:624–629